Supplementary Information

Engineering Trace AuNPs on Monodispersed Carbonized Organosilica Microspheres Drives High-Efficient and Low-Cost Solar Water Purification

Ranran Cui,[a] Jilei Wei,[a] Cui Du,[a] Shasha Sun,[b] Chen Zhou,[c] Huaiguo Xue[a] and Shengyang Yang*[a]

[a] Department of Chemistry and Chemical Engineering, Yangzhou University, Yangzhou 225002, P. R. China.

[b] School of Environmental and Chemical Engineering, Jiangsu University of Science and Technology, Zhenjiang 212005, P. R. China.

[c] School of Natural Sciences, University of Central Missouri, Warrensburg, Missouri 64093, USA.

* Corresponding authors. Email: syyang@yzu.edu.cn (S. Yang)

Experimental Section

Synthesis of monodispersed organosilica microspheres (OSMS).

1 g of trimethoxysilylpropanethiol (TMST) was slowly dropped into DI water (250 mL) under mechanical stirring for 1 h. After that, 3.5 mL of $NH_3 \cdot H_2O$ (28 wt%) was gradually added into the above solution with continuous stirring for 12 h. The solution was centrifuged and repeatedly washed with DI water to obtain organosilica microspheres (OSMS), which were then dried under vacuum for further use.

Fabrication of AuNPs@c-silica microspheres.

0.25 g of dried OSMS were dispersed in 25 mL of DI water by sonication. After that, 0.1 mL of $HAuCl_4$ solution (0.25 M) was added into the solution with sonication at room temperature for 1 h in the absence of light. Through this step, the Au ions were graft onto organosilica microspheres via the interaction between -SH group and Au^{3+}. Subsequently, the organosilica microspheres containing Au ions were obtained by centrifuge and wash. Finally, the AuNPs@c-silica was obtained by annealing Au-grafted organosilica microspheres at 800 °C for 6 h under Ar flow.

To tune the Au content on organosilica microspheres, 0 mL, 0.05 mL, 0.2 mL, and 0.4 mL of $HAuCl_4$ solutions (0.25 M) were utilized, respectively. The other conditions are identical in the whole process. Note: the superfluous $HAuCl_4$ in solution was recycled via freeze-drying.

Preparation of AuNPs@c-silica/filter fiber paper (FFP) (GSP) membrane.

To prepare AuNPs@c-silica/FFP (GSP) membrane, 40 mg of AuNPs@c-silica microspheres was homogeneously dispersed in 40 mL DI water under sonication. After that, the solution was gradually dropped onto FFP (3.5*4 cm) by filtration under mild negative pressure conditions.

With the ICP-OES results, the Au content in GSP membranes was calculated to be about 19, 25, 40, and 53 μg cm^{-2} and the corresponding membranes were denoted as GSP0, GSP, GSP1, GSP2, respectively.

For the preparation of the c-silica/FFP (SP) membrane, carbonized OSMS without Au loading was used to replace AuNPs@c-silica.

Solar water evaporation and water purification with the GSP membrane.

The water evaporation and water purification experiments were carried out in a quartz beaker with 100 mL pure water, seawater, or contaminated water under one sun irradiation (1 kW m^{-2}) with an AM 1.5 G filter. In addition, all experiments were conducted in a closed room with a temperature of ~24 °C and the humidity of ~65%. The water weight change was measured by a balance with an accuracy of 0.1 mg. To collect water, the quartz beaker was put in a glass tank and enclosed with a quartz lid.

Characterizations.

Scanning electron microscopy (SEM) images were obtained with a GeminiSEM 300 field emission scanning electron microscope system (Carl Zeiss). Transmission electron microscopy (TEM) and chemical element mapping analysis were performed on a field emission transmission electron microscope (Tecnai G2F30S-TWIN, FEI) at an acceleration voltage of 300 kV. The X-ray photoelectron spectroscopy (XPS) data were acquired with an electron spectrometer (ESCALAB250 Xi, Thermo Fisher). The X-ray diffraction (XRD) pattern was obtained with an X-ray diffractometer (D8 Advance, BRUKER-AXS) utilizing Cu Kα radiation. The Brunauer-Emmett-Teller (BET) specific surface area (SBET) was measured by nitrogen adsorption-desorption isotherm measurements (ASAP 2020 HD88, icromeritics). The concentration of methyl orange, methylene blue, and rhodamine B was detected by high-performance liquid chromatographic (HPLC, 1260, Agilent). The metal ion concentrations were measured by an inductively coupled plasma emission spectrometer (Optima 8300, PerkinElmer). The Fourier transform infrared spectra (FT-IR) was measured by using KBr pellets on a Bruker spectrometer (Tensor 27, Bruker). The thermal conductivity and thermal diffusion coefficient were measured by a hot disk thermal constants analyzer (TPS-2500, Hot Disk). The solid UV-vis diffuse reflectance spectra were measured by using a UV-Vis-NIR spectrophotometer (Cary-5000, Varian) from 2500 to 200 nm and the liquid UV-vis spectra were obtained by UV-vis spectroscopy (i5, Hanon). A digital camera (COOLPIX S8100, Nikon) was used for obtaining

photographs. The thermal imaging of Digital infrared was taken by a thermal infrared imager (testo 869, testo).

Determination of Au content in the AuNPs@c-silica.

10 mg of AuNPs@c-silica sample was added into aqua regia under sonication and heat for over 12 h. The solution was then centrifuged and diluted for the measurement with the inductive coupling plasma atomic emission spectrometry (ICP-OES).

The results show the Au content is 0.66%, 0.86%, 1.39%, and 1.85% in AuNPs@c-silica hybrid when 0.05 mL, 0.1 mL, 0.2 mL, and 0.4 mL of $HAuCl_4$ solutions (0.25 M) were utilized, respectively.

Recycle of AuNPs@c-silica

The GSP membrane was repeatedly placed in a proper amount of water under intense sonication until the membrane became white. The water containing AuNPs@c-silica was centrifuged and the precipitates were dried under vacuum. The recycled AuNPs@c-silica nanparticles were employed to prepare a new AuNPs@c-silica/FFP (GSP) membrane with the same process of the fresh one.

Note. S1. Estimation of equivalent evaporation enthalpy and calculation of solar thermal conversion efficiency

Because the cotton cloth can enhance the water evaporation via transpiration, the actual vaporization enthalpy is lower than the latent enthalpy. To estimate the actual vaporization enthalpy, the water evaporation rate in the presence of cotton cloth and GSP membrane was used to compare with pure water evaporation rate under the same conditions. The experiment was conducted under a dark environment to avoid the influence of light. Consequently, the actual evaporation enthalpy (h_{lv}) can be estimated by[1]:

$$h_{lv} = \frac{h_0}{m_r} \tag{1}$$

where h_0 represents the evaporation enthalpy of water at the corresponding temperature, m_r is the mass change ratio of water in the presence of membranes and bulk water.

With the equivalent evaporation enthalpy, the solar thermal conversion efficiency of the GSP membrane and other membranes can be obtained as follows

Parameters	H_2O	FFP	SP	GSP0	GSP	GSP1	GSP2
Evaporation rate under dark (g m^{-2} h^{-1})	18.63	27.9	20.6	20.5	20.7	20.7	20.6
m_r	1	1.49	1.106	1.10	1.11	1.11	1.106
h_0 (kJ kg^{-1})	2432	2437	2396	2394	2388	2390	2392
h_{lv} (kJ kg^{-1})	2432	1633	2166	2176	2151	2153	2163
Evaporation rate (kg m^{-2} h^{-1})	0.39	0.47	1.11	1.23	1.50	1.40	1.39
Increased temperature (K)	6.2	10.7	25	24.8	29.2	26.3	25.8
Efficiency (%)	26.62	21.9	70	77.9	94.6	87.9	87.6

Note. S2. Simulation of light-to-heat conversion via COSMOL

Because the densities of graphite carbon and amorphous silica are all close to 2.2 g cm^{-3} and the Au content in AuNPs@c-silica is limited, we presumed the density of AuNPs@c-silica is 2.2 g cm^{-3}. The diameters of AuNPs and AuNPs@c-silica were set to 4 nm and 400 nm, respectively. With the ICP-OES result, the Au content is about 0.86%, we can calculate the number of AuNPs by the formula

$$\text{Mass Percentage (\%)} = \frac{n \times \rho_{AuNPs} \times \frac{4}{3}\pi R^3_{AuNPs}}{\rho_{AuNPs@c\text{-}silica}\frac{4}{3}\pi R^3_{AuNPs@c\text{-}silica} + n \times \rho_{AuNPs} \times \frac{4}{3}\pi R^3_{AuNPs}} = 0.86\% \quad (2)$$

The calculated number of AuNPs is 988, which was rounded to 1000 in this work.

Given a similar photothermal phenomenon between c-silica and graphite carbon (Supplementary Fig. 21), the AuNPs@c-silica was replaced with s-AuNPs@carbon, which represents 1000 of 4 nm AuNPs were homogenously distributed on carbon sphere (400 nm).

For the simulation of light-to-heat and heat transfer, the wave equation and heat equation were utilized.

Table S1. The cost of the GSP membrane estimated with the industrial product cost.

Material	Price	Material Consumption	Price/Device
$HAuCl_4$	\$33.42 (1 g)	0.25 g (AuNPs)	\$17.48
$NH_3 \cdot H_2O$	\$0.3 (1 kg)	~123 g	\$0.037
TMST	\$4.89 (1 kg)	~35 g	\$0.17
FFP	\$7 (10 m^2)	1 m^2	\$0.7
Cost of GSP			\$18.39 m^{-2}

Table S2. The cost of the ideal GSP membrane estimated with the industrial product cost.

Material	Price	Material Consumption	Price/Device
$HAuCl_4$	\$33.42 (1 g)	7.8 mg (AuNPs)	\$0.545
$NH_3 \cdot H_2O$	\$0.3 (1 kg)	~1.97 g	\$0.0006
TMST	\$4.89 (1 kg)	~0.56 g	\$0.003
FFP	\$7 (10 m^2)	1 m^2	\$0.7
Cost of GSP			\$1.25 m^{-2}

Table S3. The photothermal conversion efficiency of the GSP membrane compared with other Au-involved membranes[2-10].

Membrane Materials	Conditions			Rate (kg m^{-2} h^{-1})	Efficiency (%)	Ref.
	Light Intensity (kW m^{-2})	Temperature (°C)	Humidity (%)			
AuNPs@c-silica/FFP	1	24	~65	1.5	94.6	This work
AuNPs/Al_2O_3	1	24	~42	~0.8	59	R2
	4	24	~42	5.6	90	
Paper-based AuNP film (PGF)	4.5	NA	NA	NA	77.8	R3
AuFs	1	30	70	1.356	85	R4
Au nanostar	1	RT*	NA	1.3	83.3	R5
Au nanosphere	1	RT*	NA	1.08	68.6	R5
AuNPs/Paper	1	NA	NA	1.18	76	R6
	2.3	NA	NA	~2.88	87	
black gold membranes	20	NA	NA	15.95	57	R7
PdNPs/Wood	1	NA	NA	~1.0	~67	R8
	10	NA	NA	11.8	85	
AuNPs/MRS(BDS)	1	NA	NA	1.24	85	R9
	10	NA	NA	12.72	~90	
Pt/Au/TiO_2 -wood carbon	10	NA	NA	NA	90.4	R10

*RT: room temperature

Table S4. The ICP results of simulated seawater before and after purification with GSP membrane under one sun irradiation.

Ion	Salt Water (mg L^{-1})	WHO (mg L^{-1})	Steamed Water (mg L^{-1})	Rejection Efficiency (%)
Na^+	10860	≤200	0.7217	99.99
Mg^{2+}	1581	/	0.1909	99.99
K^+	406.6	/	0.218	99.95
Ca^{2+}	431.6	/	0.5517	99.87
Total	13279.2		1.6877	99.99

Table S5. High-performance liquid chromatographic (HPLC) results of water samples containing dyes before and after solar purification with GSP membrane.

Dyes	Stock Solution (mg L^{-1})	Steamed Water (mg L^{-1})	Rejetion Eficiency (%)
Rhodamine B	100	0.26	99.74
Methyl orange	100	0.32	99.68
Methylene blue	100	0.10	99.90

Table S6. The ICP results of polluted water containing heavy metal ions before and after purification using GSP membrane under one sun irradiation.

Ion	Stock Solution (mg L^{-1})	WHO (μg L^{-1})	Steamed Water (μg L^{-1})	Rejection Efficiency (%)
Cr^{2+}	104.2	50 (Cr^{6+})	46.58	99.96
Cd^{2+}	104.8	3	2.02	99.99
Pb^{2+}	100.1	10	6.14	99.99

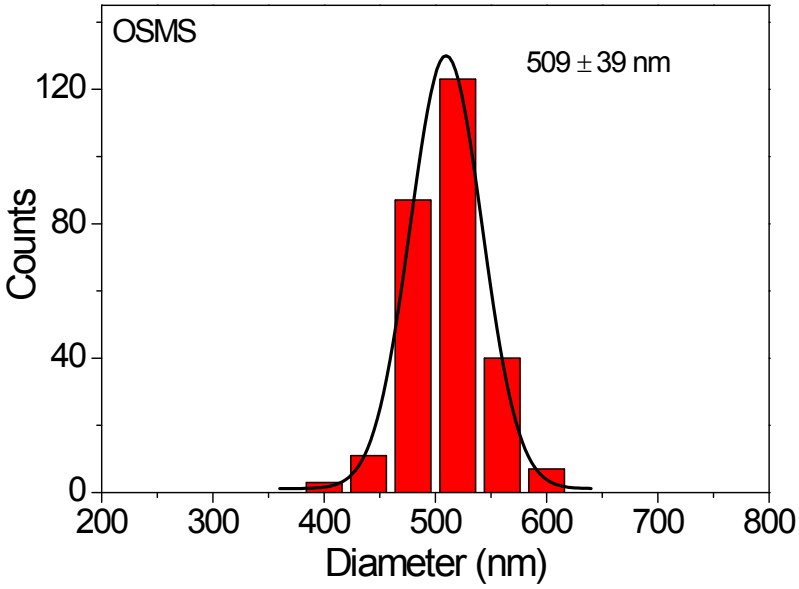

Fig. S1. The statistical diameter of OSMS from SEM images.

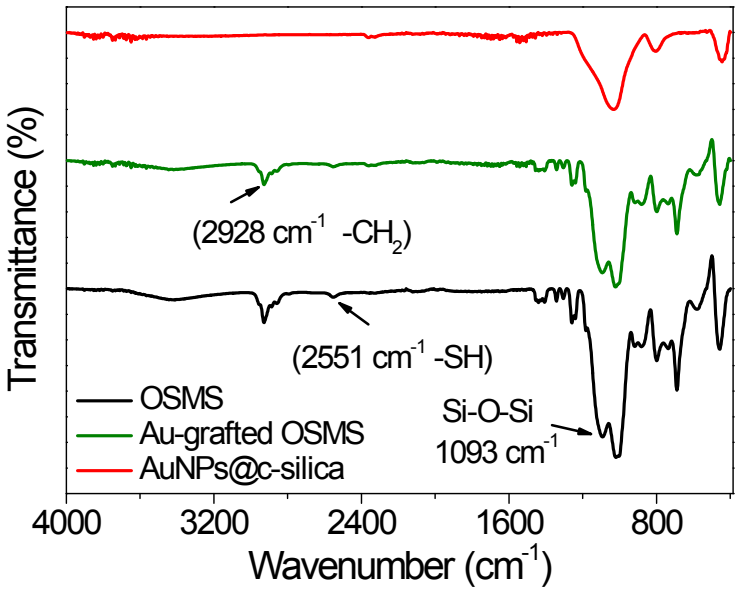

Fig. S2. FT-IR spectra of OSMS, Au-grafted OSMS, and AuNPs@c-silica.

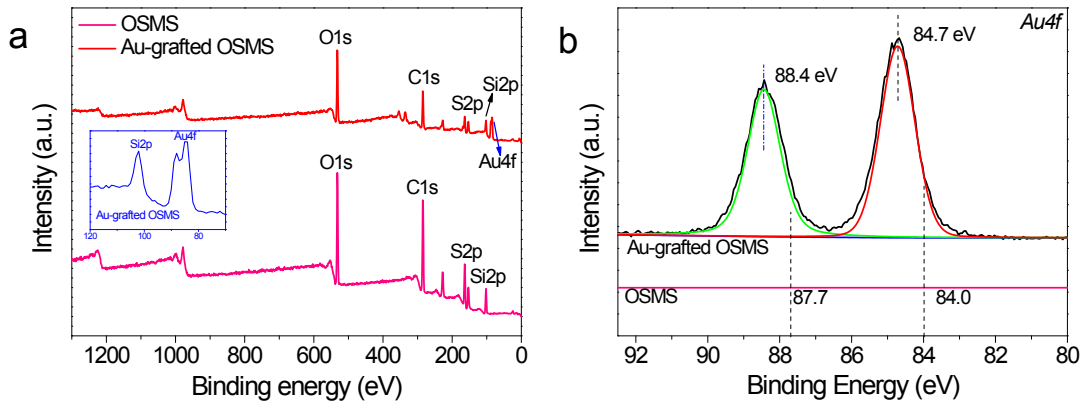

Fig. S3. (a) Survey XPS spectra of OSMS and Au-grafted OSMS. Inset: the magnification of Au XPS peaks. (b) The high-resolution Au 4f XPS spectra of Au-grafted OSMS and the standard Au 4f XPS peaks of zero valence Au. In contrast to Au^0, the Au 4f XPS peaks of Au-grafted OSMS shift to high energy, confirming the Au is an ionic state.

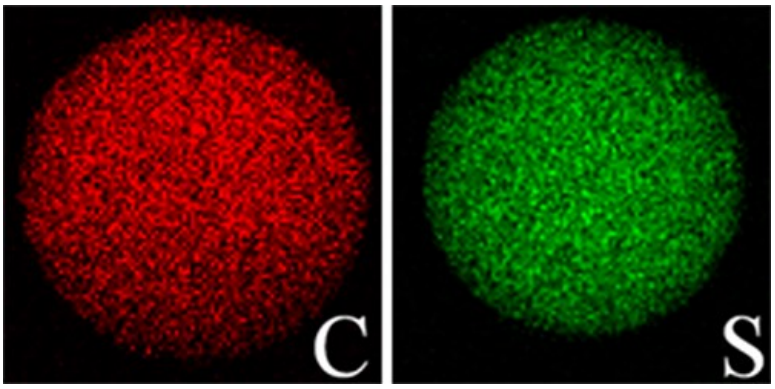

Fig. S4. EDS element distribution maps of C and S in Au-grafted OSMS.

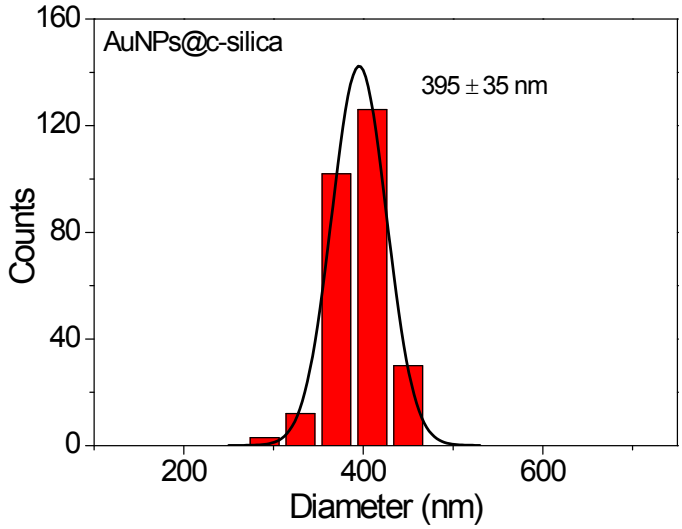

Fig. S5. The statistical diameter of AuNPs@c-silica from SEM images.

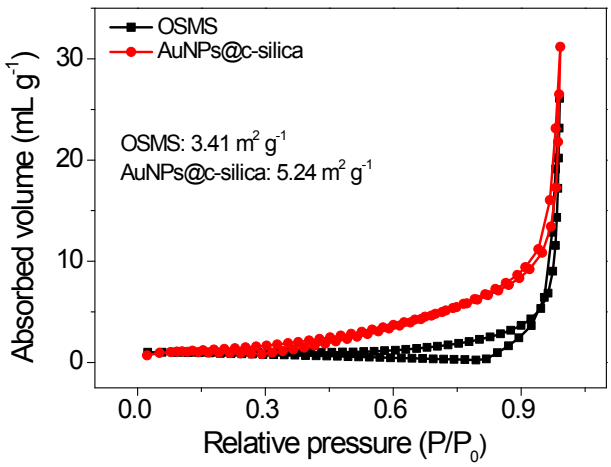

Fig. S6. Nitrogen adsorption and desorption curves of OSMS and AuNPs@c-silica.

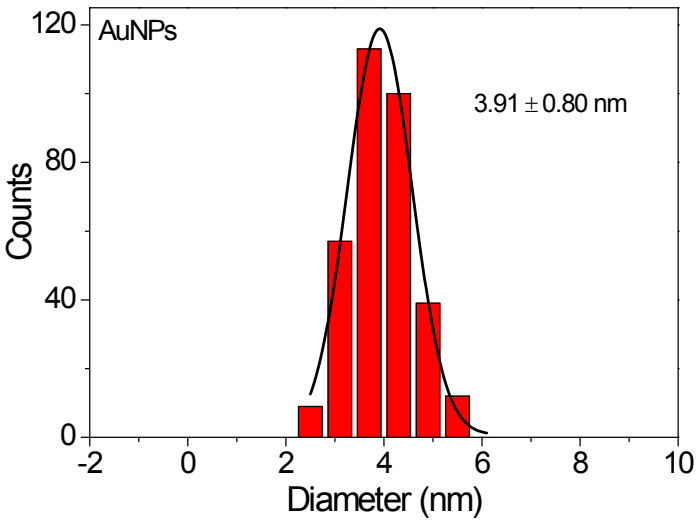

Fig. S7. The statistical diameter of AuNPs on c-silica from TEM images.

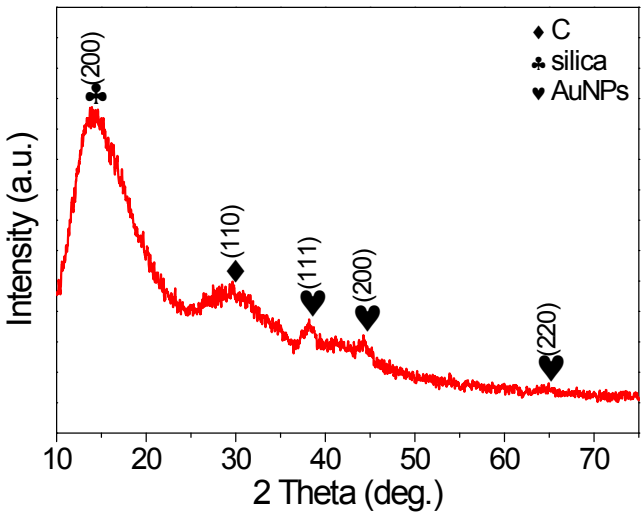

Fig. S8. The XRD pattern of AuNPs@c-silica, indicating the sample contains SiO_2 (PDF No. 32-0993), AuNPs (PDF No. 04-0784), and carbon (PDF No. 54-0501).

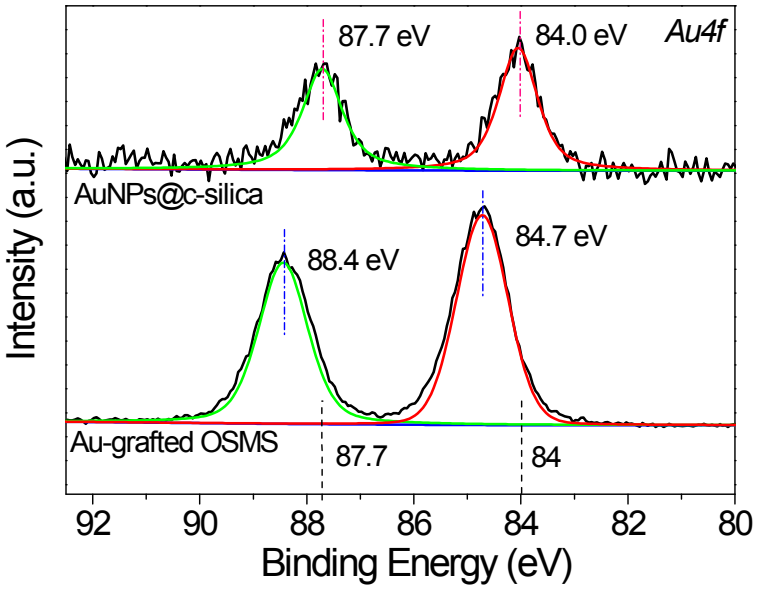

Fig. S9. High-resolution Au 4f XPS of Au-grafted OSMS and AuNPs@c-silica.

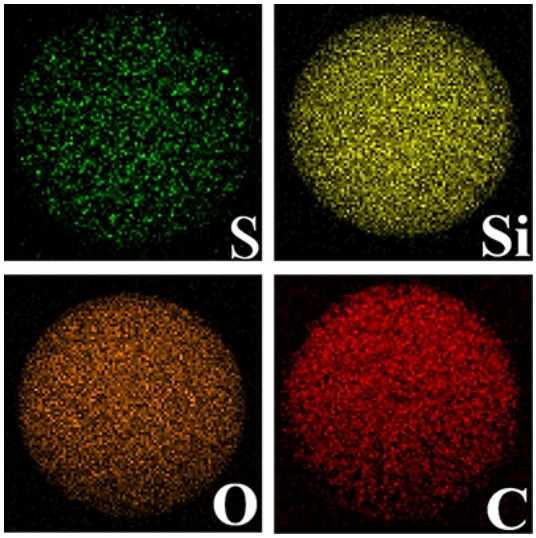

Fig. S10. EDS element distribution maps of S, Si, O, and C in AuNPs@c-silica.

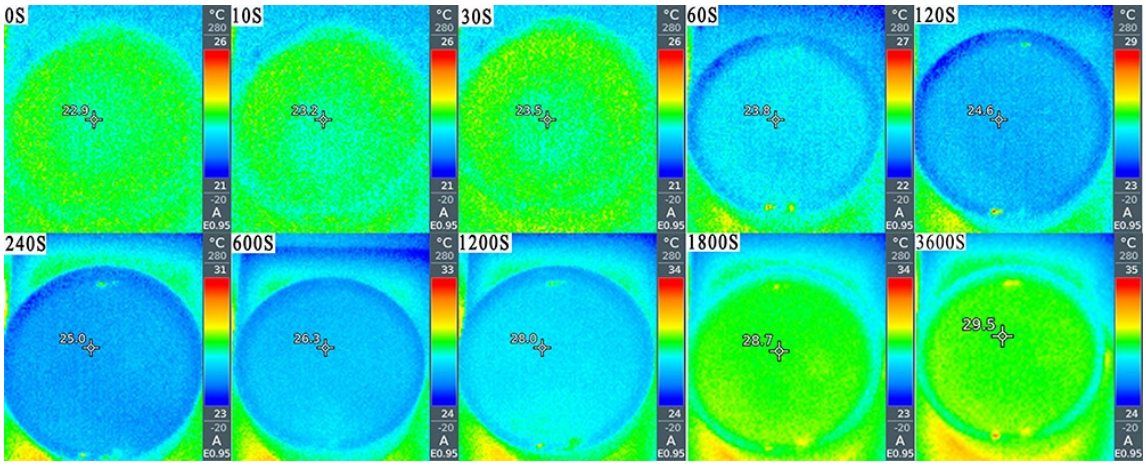

Fig. S11. Digital infrared thermal images of pure water under one sun irradiation.

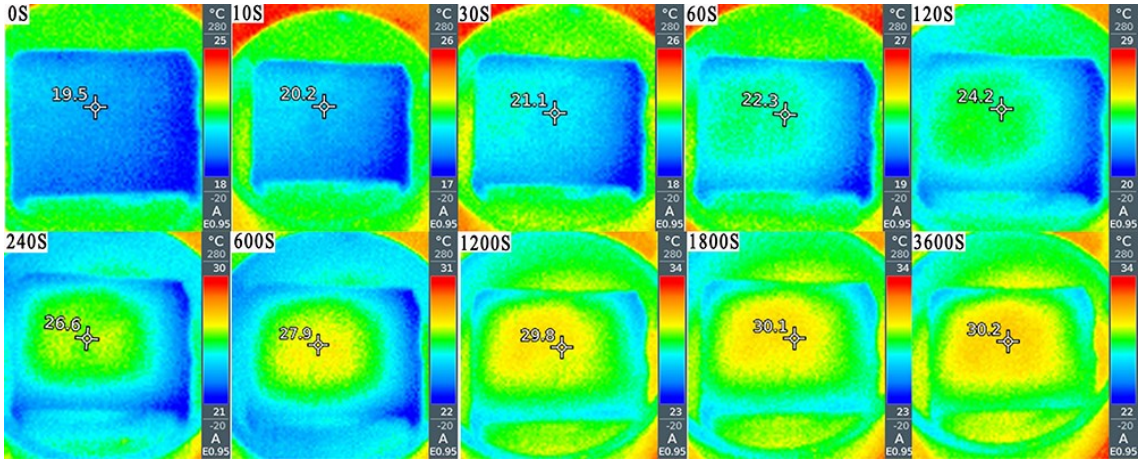

Fig. S12. Digital infrared thermal images of pure water with FFP under one sun irradiation.

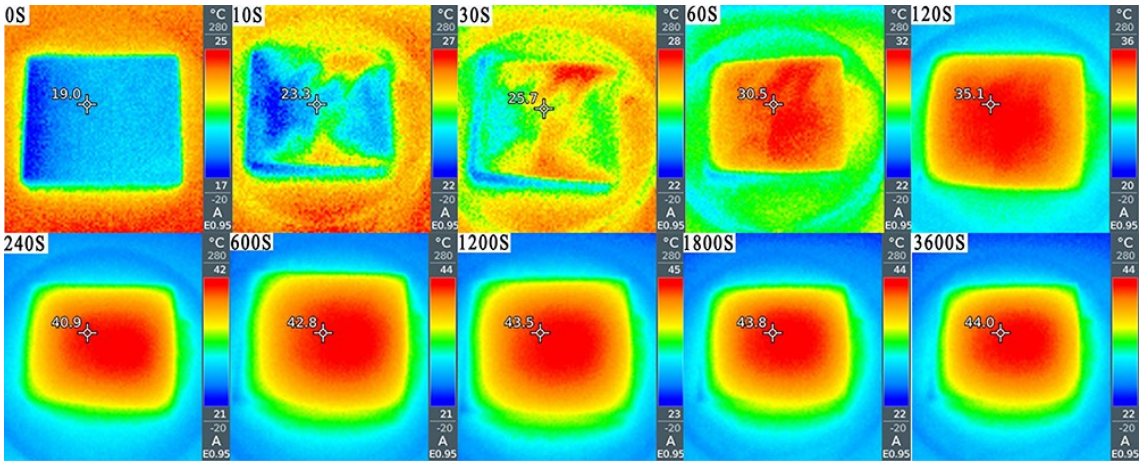

Fig. S13. Digital infrared thermal images of pure water with SP membrane under one sun irradiation.

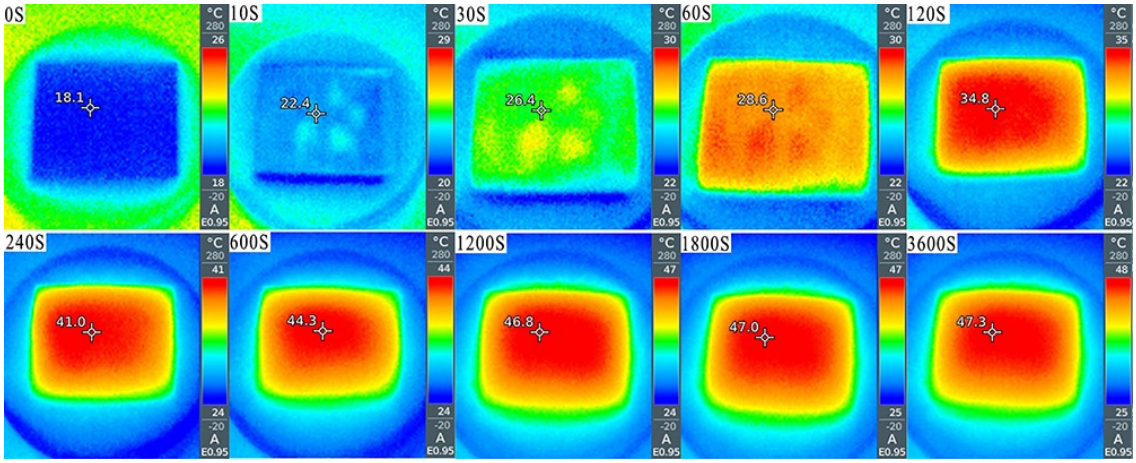

Fig. S14. Digital infrared thermal images of pure water with GSP membrane under one sun irradiation.

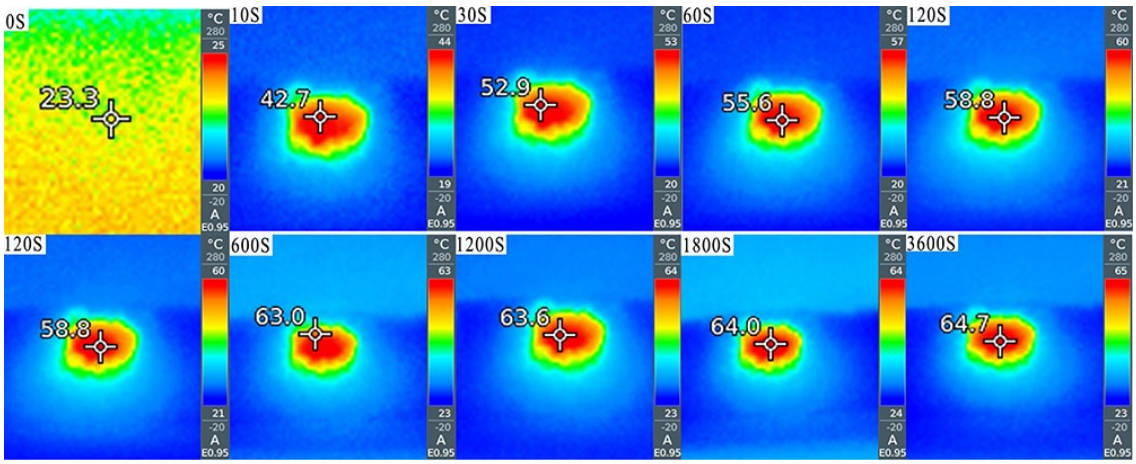

Fig. S15. Digital infrared thermal images of GSP membrane in the air under one sun irradiation. Note: the FFP will wrinkle at high temperature, so a small piece of GSP was used in the irradiation process.

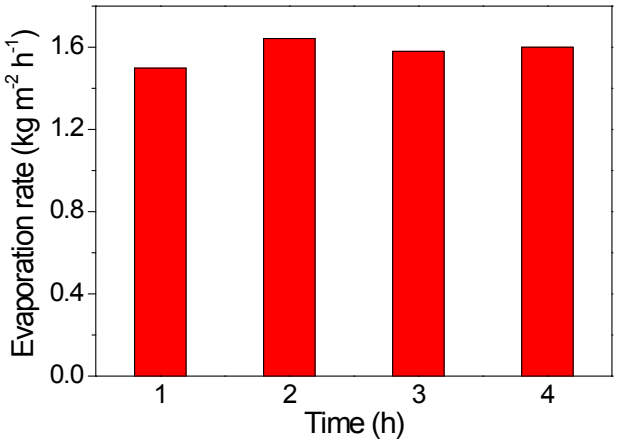

Fig. S16. The water evaporation rates with the GSP membrane versus time. In the first hour, solar energy was partially used to raise the water temperature, leading to the water evaporation rate (1.50 kg m^{-2} h^{-1}) and solar steam efficiency is relatively low (89.5%). In the following time, the temperate of water was invariant and the sensible enthalpy can be ignored under this condition. Thus, the water evaporation rate slightly increases and the average solar steam efficiency (2-4 h) is up to 95.9%, which is close to the solar thermal conversion efficiency in the first hour (94.6%).

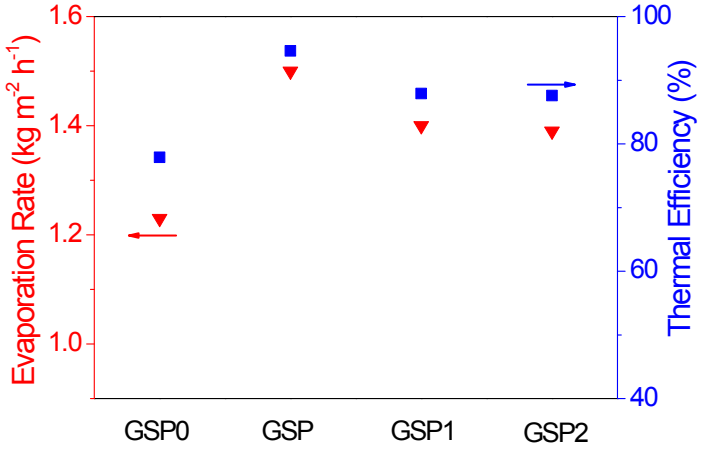

Fig. S17. Water evaporation rate and photothermal conversion efficiency of GSP0, GSP, GSP1, and GSP2 membranes under 1 sun for 1 h irradiation.

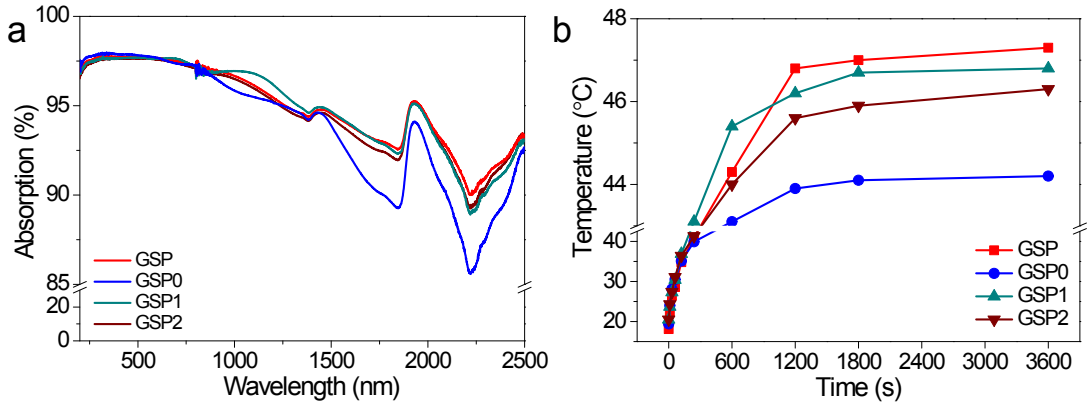

Fig. S18. (a) The absorptions of GSP, GSP0, GSP1, and GSP2 membranes. (b) The temperature curves of GSP, GSP0, GSP1, and GSP2 membranes on the water surface under 1 sun for 1 h irradiation.

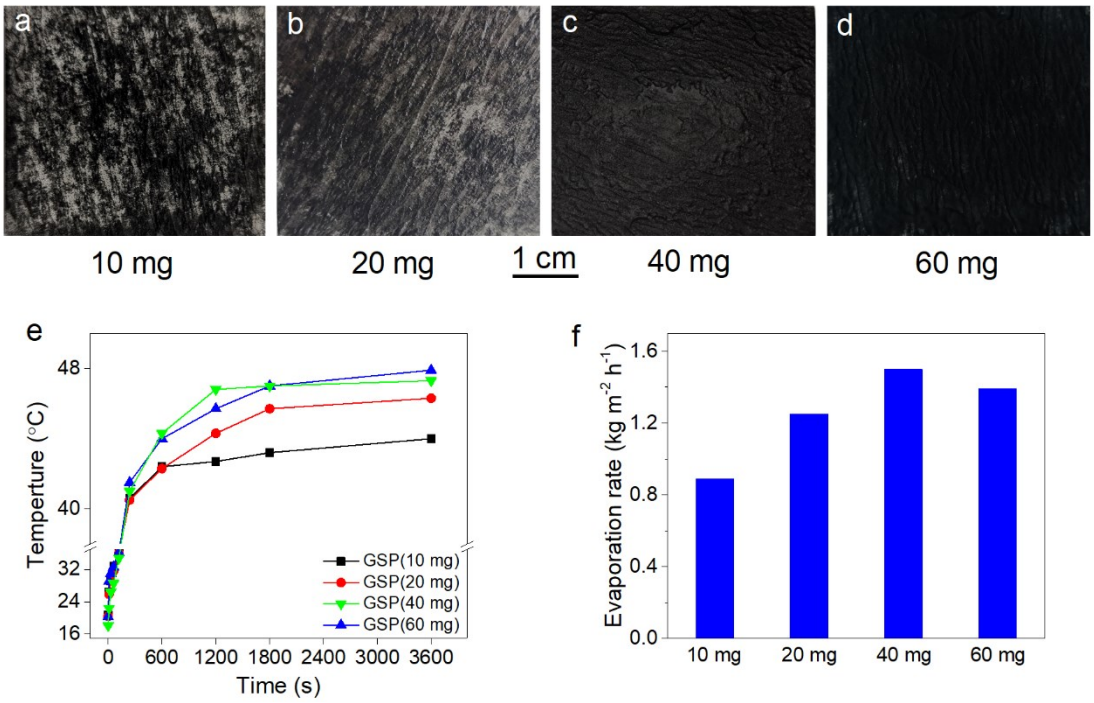

Fig. S19. (a-d) The photographs of the GSP membranes with loading different amounts of AuNPs@c-silica. (e) The temperature curves of the GSP membranes with loading different amounts of AuNPs@c-silica on the water surface under 1 sun for 1 h irradiation. (f) Water evaporation rate of GSP membranes with loading different amounts of AuNPs@c-silica under 1 sun for 1 h irradiation.

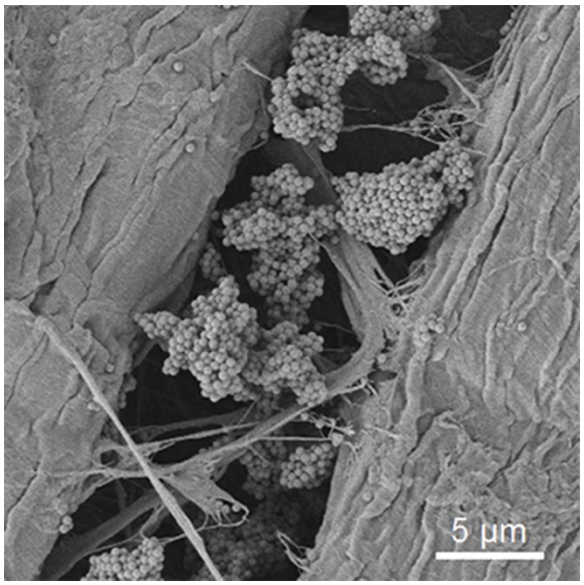

Fig. S20. SEM images of the GSP membrane.

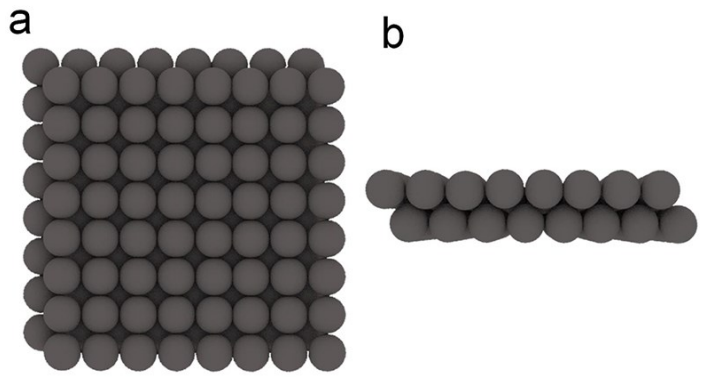

Fig. S21. The AuNPs@c-silica microspheres are orderly arrayed with double layers under ideal conditions, (a) top view, (b) lateral view. The corresponding Au content in the ideal membrane is evaluated as

$$\text{Mass (m}^{-2}) = \rho nNVr = 2.2 \times 2 \times \frac{10^{14}}{395^2} \times \frac{4 \times 395^3 \pi}{3 \times 2^3 \times 10^{21}} \times 0.86\% = 7.82 \text{ mg m}^{-2} \quad \text{(S3)}$$

where ρ is the density of AuNPs@c-silica (estimated as 2.2 g cm^{-3}, please see experimental part); *n* is equal to 2, indicating double layers; *N* is the number of AuNPs@c-silica on one square centimeter; *V* is the volume of AuNPs@c-silica (cm^3); and *r* is the mass ratio of Au in AuNPs@c-silica (determined by ICP-OES).

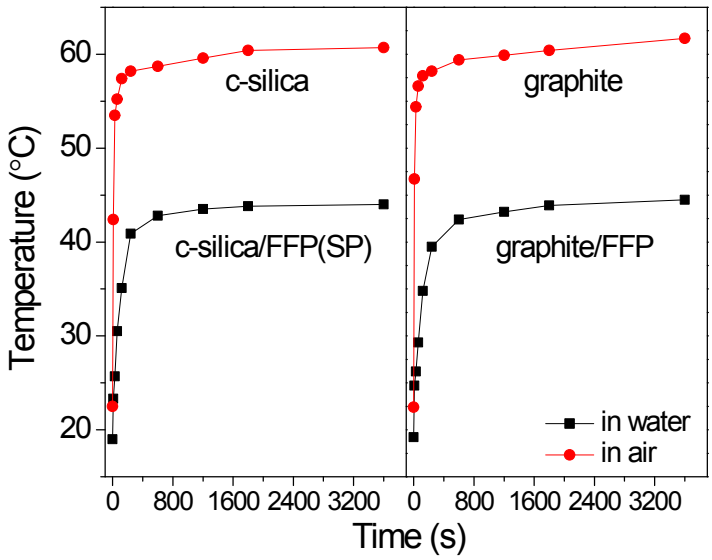

Fig. S22. The temperature curves of c-silica and graphite carbon in air and the membranes of FFP loading the same amount of c-silica or graphite carbon on water surface under 1 sun for 1 h irradiation.

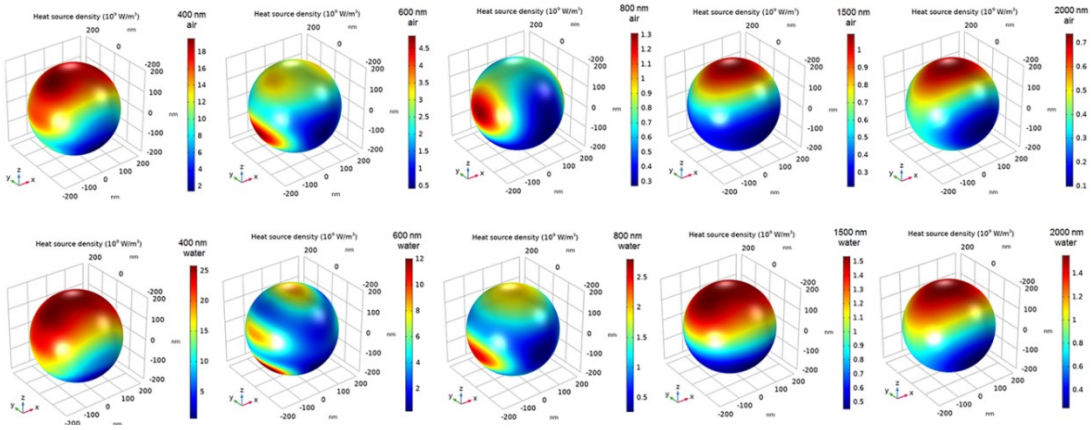

Fig. S23. The simulated point heat source densities (PHSD) of large AuNP under different wavelengths in the air (top) and water (bottom) with a light intensity of 100 mW cm^{-2}.

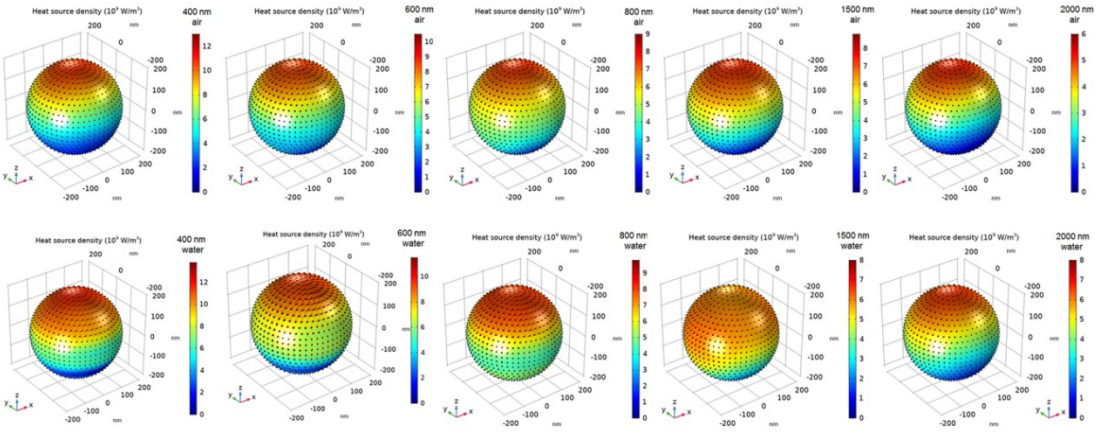

Fig. S24. The simulated point heat source densities (PHSD) of s-AuNPs@carbon under different wavelengths in the air (top) and water (bottom) with a light intensity of 100 mW cm^{-2}.

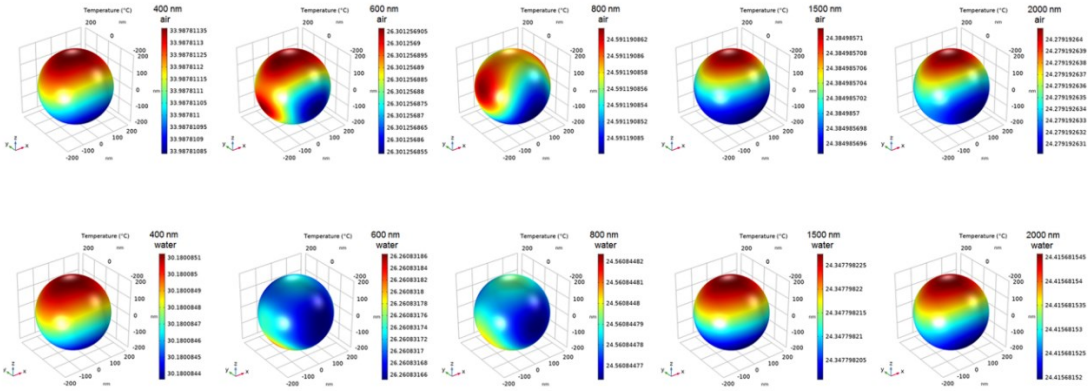

Fig. S25. The simulated surface temperature of large AuNP under different wavelengths in the air (top) and water (bottom) with a light intensity of 100 mW cm^{-2}.

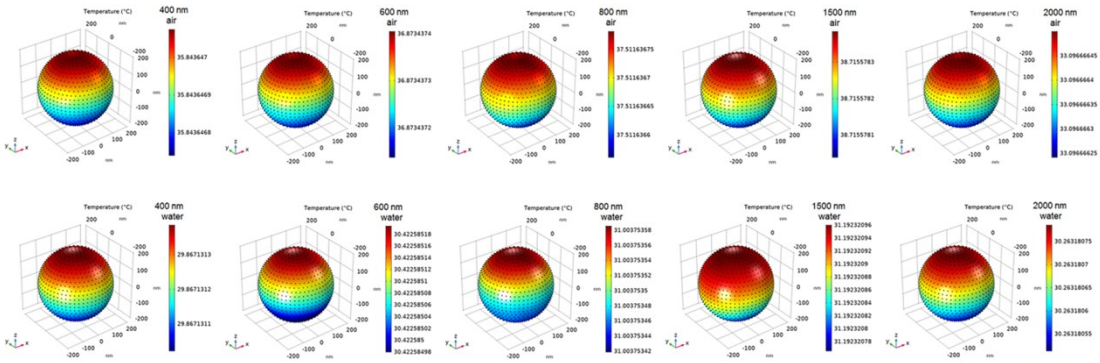

Fig. S26. The simulated surface temperature of s-AuNPs@carbon under different wavelengths in the air (top) and water (bottom) with a light intensity of 100 mW cm^{-2}.

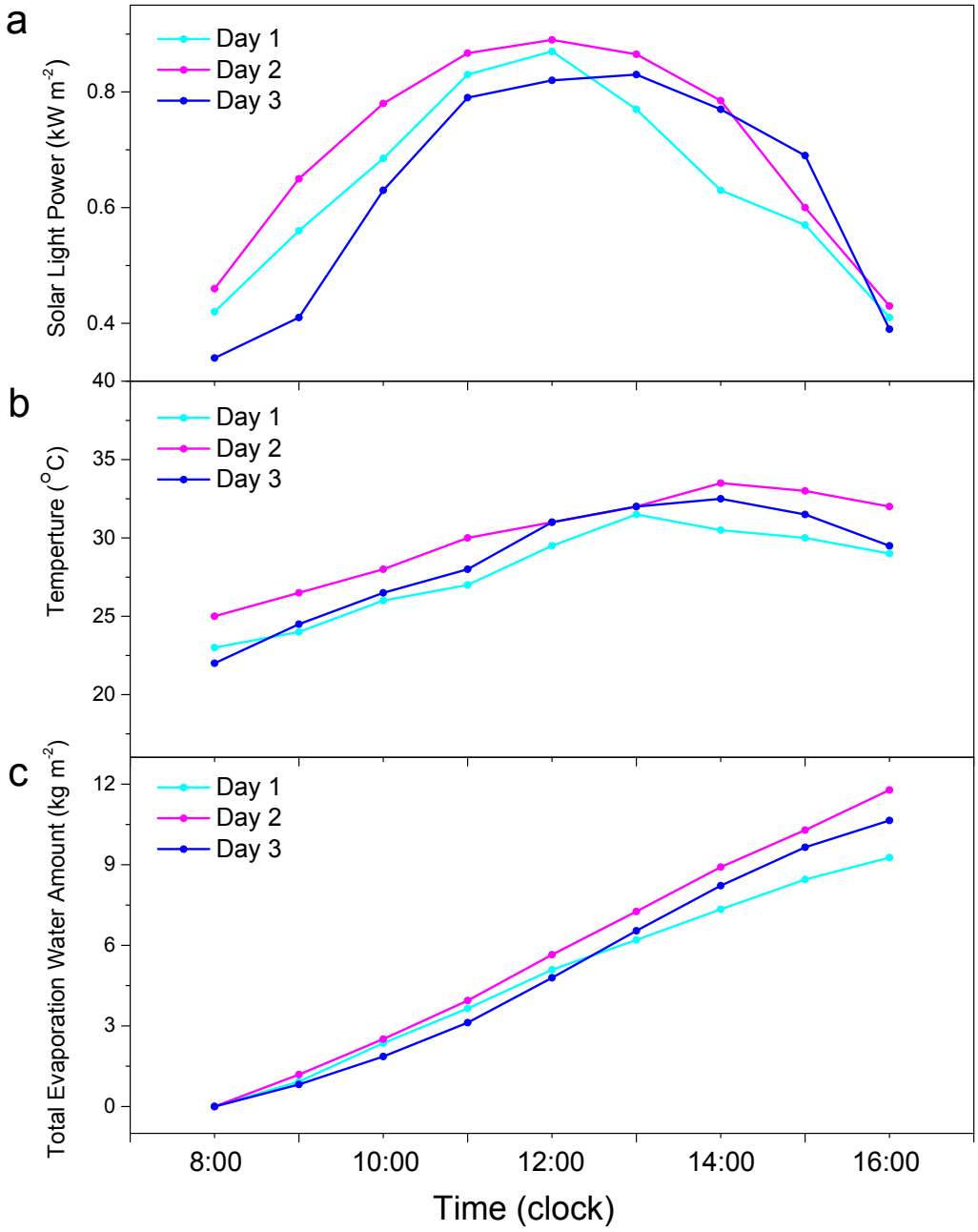

Fig. S27. (a) The solar light power under the natural sunlight from 8:00 am to 4:00 pm. (b) The air temperature curves of the environment from 8:00 am to 4:00 pm. (c) The total evaporation water amounts from 8:00 am to 4:00 pm. (open system, gentle breeze).

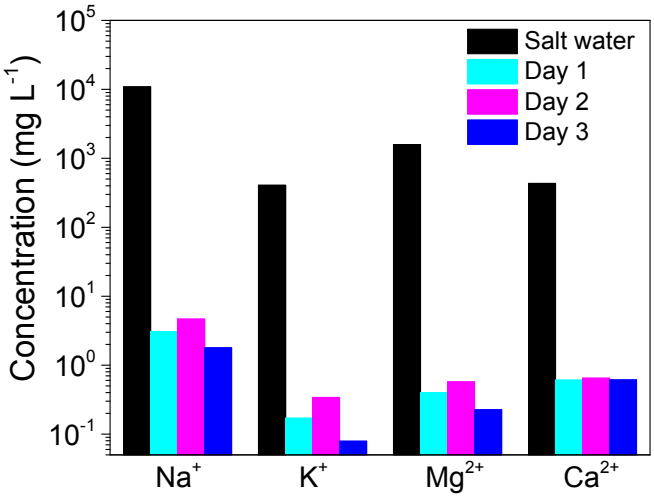

Fig. S28. The ion concentrations of simulated seawater before and after outdoor solar photothermal purification with GSP membrane.

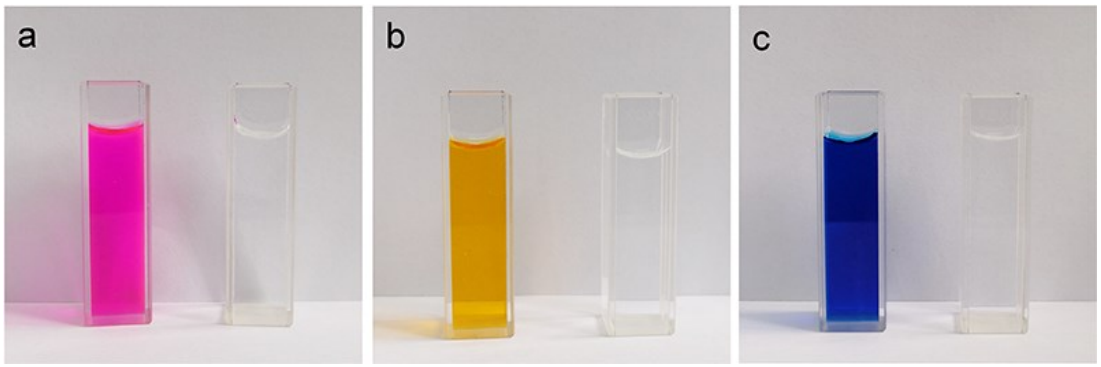

Fig. S29. The photographs of contaminated water (a: rhodamine B, b: methyl orange, and c: methyl blue, 100 mg L^{-1}) before and after solar purification with the GSP membrane.

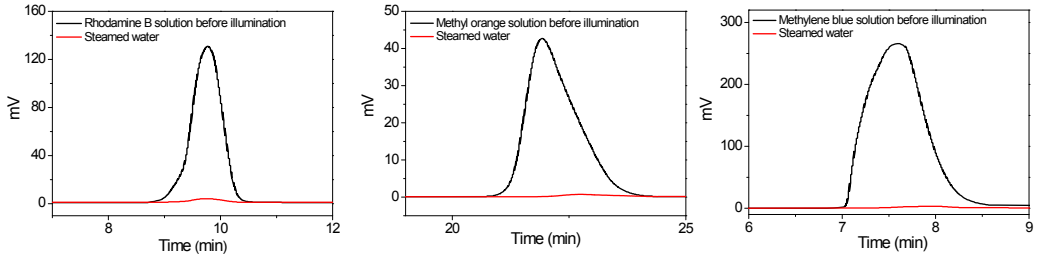

Fig. S30. The HPLC spectra of dye-contaminated water before and after solar purification with the GSP membrane.

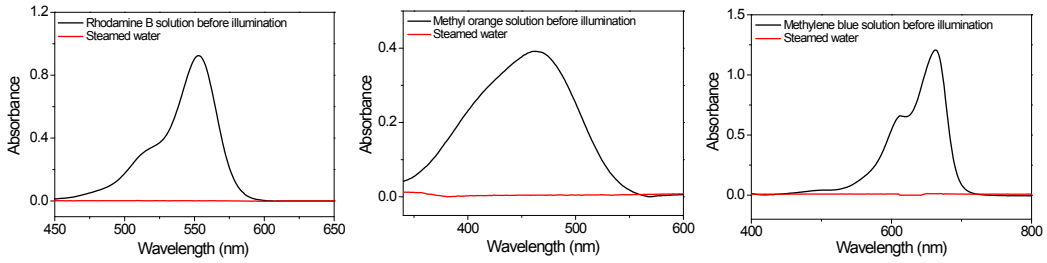

Fig. S31. The UV-vis absorption spectra of dye-contaminated water before and after solar purification with the GSP membrane.

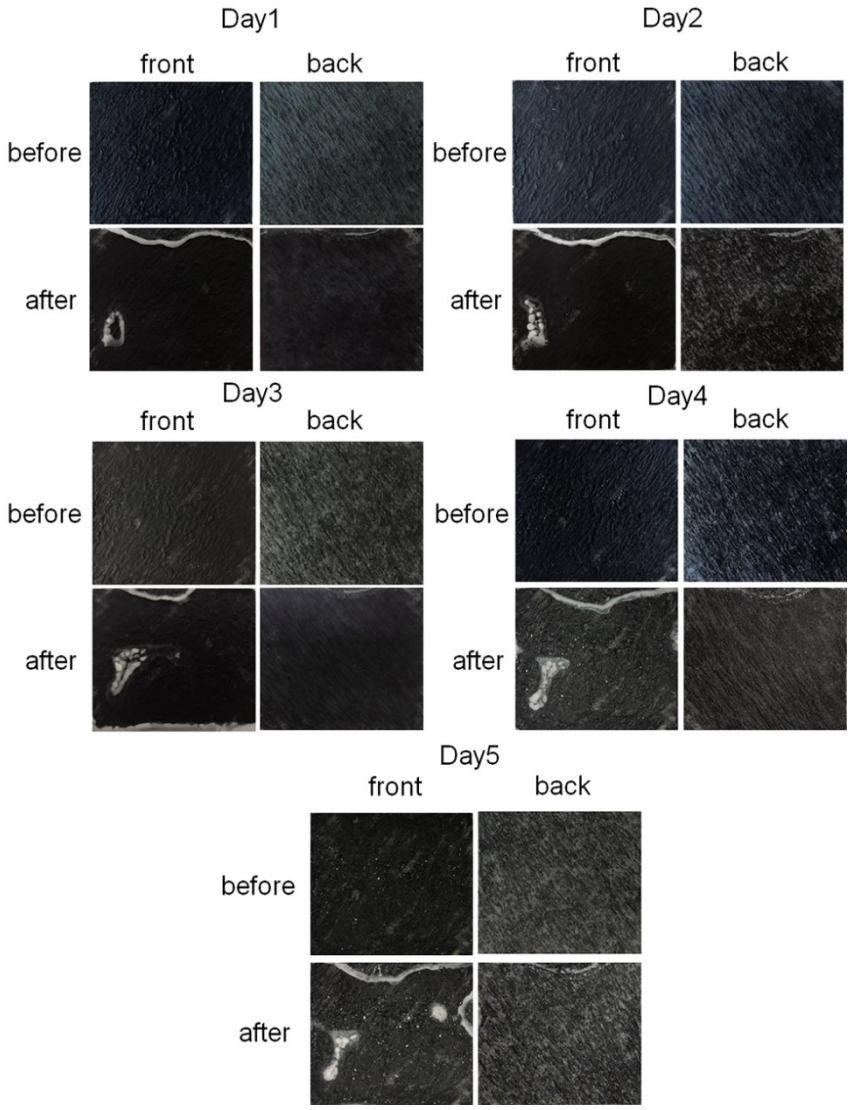

Fig. S32. The front and back photographs of the GSP membrane before and after solar seawater evaporation for recycling 5 days.

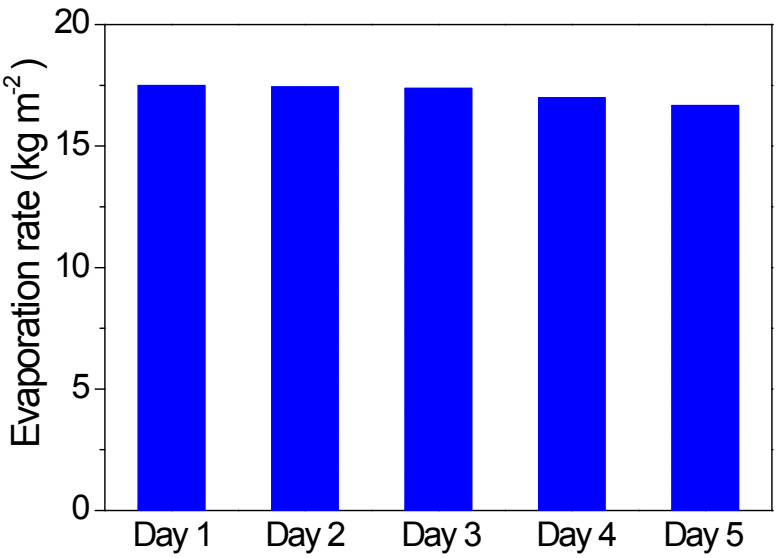

Fig. S33. The seawater evaporation amount with the GSP membrane under one sun irradiation for 12 h per day.

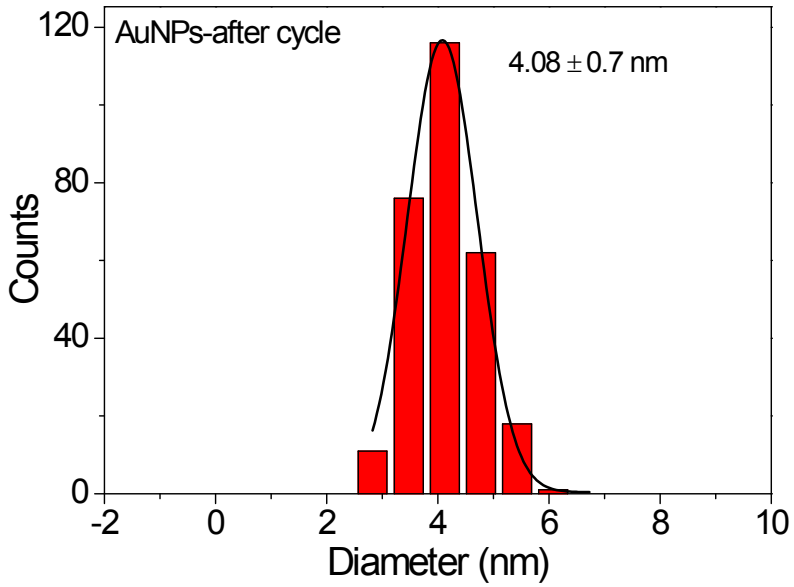

Fig. S34. The statistical diameter of AuNPs on c-silica from TEM images after the seawater desalination for 5 days.

Supplementary References

[1] Y. Guo, F. Zhao, X. Zhou, Z. Chen and G. Yu, *Nano Lett.*, 2019, **19**, 2530-2536.

[2] L. Zhou, Y. Tan, D. Ji, B. Zhu, P. Zhang, J. Xu, Q. Gan, Z. Yu and J. Zhu, *Sci. Adv.*, 2016, **2**, e1501227.

[3] Y. Liu, S.Yu, R. Feng, A. Bernard, Y. Liu, Y. Zhang, H. Duan, W. Shang, P. Tao, C. Song, T. Deng, *Adv. Mater.*, 2015, **27**, 2768-2774.

[4] M. Gao, C. K. Peh, H. T. Phan, L. Zhu and G. W. Ho, *Adv. Energy Mater.*, 2018, **8**, 1800711.

[5] G. Song, Y. Yuan, J. Liu, Q. Liu, W. Zhang, J. Fang, J. Gu, D. Ma and D. Zhang, *Adv. Sustainable Syst.*, 2019, **3**, 1900003.

[6] C. Liu, J. Huang, C.-E. Hsiung, Y. Tian, J. Wang, Y. Han and A. Fratalocchi, *Adv. Sustainable Syst.*, 2017, **1**, 1600013.

[7] K. Bae, G. Kang, S. K. Cho, W. Park, K. Kim and W. J. Padilla, *Nat. Commun.*, 2015, **6**, 10103.

[8] M. Zhu, Y. Li, F. Chen, X. Zhu, J. Dai, Y. Li, Z. Yang, X. Yan, J. Song, Y. Wang, E. Hitz, W. Luo, M. Lu, B. Yang and L. Hu, *Adv. Energy Mater.*, 2018, **8**, 1701028.

[9] Y. Liu, Z. Liu, Q. Huang, X. Liang, X. Zhou, H. Fu, Q. Wu, J. Zhang and W. Xie, *J. Mater. Chem. A*, 2019, **7**, 2581-2588.

[10] M. Wang, P. Wang, J. Zhang, C. Li and Y. Jin, *ChemSusChem*, 2019, **12**, 467-472.